GEOPHYSICS, VOL. 75, NO. 5 (SEPTEMBER-OCTOBER 2010); P. 75A139–75A146, 8 FIGS.
10.1190/1.3467760

Reservoir characterization using surface microseismic monitoring

Peter M. Duncan[1] and Leo Eisner[1]

ABSTRACT

Microseismic monitoring of reservoir processes can be performed using surface or near-surface arrays. We review the published technical basis for the use of the arrays and the historical development of the method, beginning with locating earthquakes through geothermal exploration to the growing field of hydraulic-fracture monitoring. Practical considerations for the array deployment and data processing are presented. The road ahead for the technology includes a move toward life-of-field buried arrays as well as opportunities for extended interpretation of the data, particularly inversion for source-mechanism estimation and measurement of anisotropy in the monitored subsurface.

INTRODUCTION

In a companion paper, Maxwell et al. (2010) indicate two microseismic monitoring techniques used today: surface and downhole monitoring. Both methods were anticipated by Bailey in his patent (1973) on the application of microseismic monitoring to hydraulic-fracture mapping. This paper completes the discussion begun by Maxwell et al. (2010) by addressing the current use of surface and near-surface geophone arrays for monitoring applications.

Maxwell et al. (2010) list three general classes of techniques for locating microseismic events: (1) hodogram techniques based upon the particle motion of direct arrivals, (2) triangulation schemes based upon arrival times of direct waves, and (3) semblance methods based upon stacking waves without arrival-time picking. All three classes of location techniques can be used in conjunction with surface or downhole sensors. The first two classes are usually based on discrete detection of the small signals we wish to monitor, so downhole sensor deployment is often necessary to resolve the location. On the other hand, the aperture and fold requirements of the semblance class of location techniques tend to favor a large areal spread of sensors as can be achieved most conveniently with a surface or near-surface array. Such arrays may consist of hundreds or even thousands of geophones located above the target reservoir, depending upon the required fold and the desired image area. Field operations for deploying a surface array have the look and feel of a modern 3D recording crew.

In what follows, we describe the history and current practice of surface and near-surface array reservoir monitoring as well as suggest areas of future development.

HISTORY

McMechan (1982) notes that the familiar geophysical technology known as migration could be readily applied to the problem of earthquake source imaging. He points out that in migration models of reflection data, reflectors or diffractors can be thought of as spatial distributions of secondary sources. This is also known as the exploding reflector model (Claerbout, 1985). In the case of earthquake or microseismic data, the sources distributed along the failure planes become primary rather than secondary sources. The concept of imaging these sources by wavefield extrapolation and an imaging condition still applies. McMechan tests his reverse-time imaging approach successfully on synthetic data and develops rules for sampling the wavefield, similar to those that apply in reflection imaging. McMechan et al. (1985) apply this technique to imaging earthquake sources in Long Valley, California, for three events that occurred in 1983. The data used to locate the earthquakes were recorded with 120 portable seismographs arranged in a somewhat linear spread over 12 km.

Kiselevitch et al. (1991) report on a slightly different approach to using surface arrays for microseismic investigations, which they term *emission tomography*. In this technique, they define a semblance measure achieved by normalizing the time average of the product of the time-shifted signals by the product of the time averages of the signals. The time shift applied is exactly the traveltime difference between the stations in the array, i.e., the moveout across the array. The length of the averaging time window is driven by the duration of the signal. Short signals require a larger signal-to-noise ratio (S/N) for the semblance measure to isolate the signal. Weak signals with a longer duration will stand out above random noise. The technique was successfully applied by Kiselevitch et al. (1991) to ex-

Manuscript received by the Editor 26 December 2009; revised manuscript received 16 April 2010; published online 14 September 2010.
[1]Microseismic Inc., Houston, Texas, U.S.A. E-mail: pduncan@microseismic.com; leisner@microseismic.com.
© 2010 Society of Exploration Geophysicists. All rights reserved.

Downloaded 05 Dec 2010 to 99.185.9.161. Redistribution subject to SEG license or copyright; see Terms of Use at http://segdl.org/

plore a hydrothermal field in Iceland using a 24-channel array with a 1000 × 600-m footprint. The microseismic tremors associated with hydrothermal flow were recorded over a 10–50-Hz band and were found to have signal durations of 60 s. This emission tomography approach can be understood in relation to McMechan's (1982) work by recognizing that the application of the time shift is the wavefield-extrapolation step, and the semblance criterion is the statement of the imaging condition.

To our knowledge, the first application of surface-array emission tomography for monitoring a hydraulic-fracture (frac) well stimulation occurred in June 2004, as reported by Duncan (2005) and Lakings et al. (2006). The well was a 3000-ft- (900-m) long, 7800-ft- (2400-m) deep horizontal completion in the Barnett Shale, Wise County, Texas. The array consisted of 97 three-component (3-C) stations at or near the surface, deployed in a regular grid over an area of 6000 × 8000 ft (1800 × 2500 m). Figure 1, taken from that work, shows the emission semblance measure for a 60-s time window during stimulation as well as the layout of the well and the seismic stations. The image represents the average seismic energy released over the 60-s time window and therefore is presumed to be the result of more than one microseismic event. To look at individual events, the time-averaging window must be reduced in length to something more representative of the time duration of the triggered microseismic events. A longer time-average image, such as the one in Figure 1, nicely conveys the areal extent of energy released over the selected time interval. The image also conveys a sense of the uncertainty in event location, in that the peak(s) of the energy contours is the most likely location of the event(s) and the width of the contoured peak is related to the event location uncertainty.

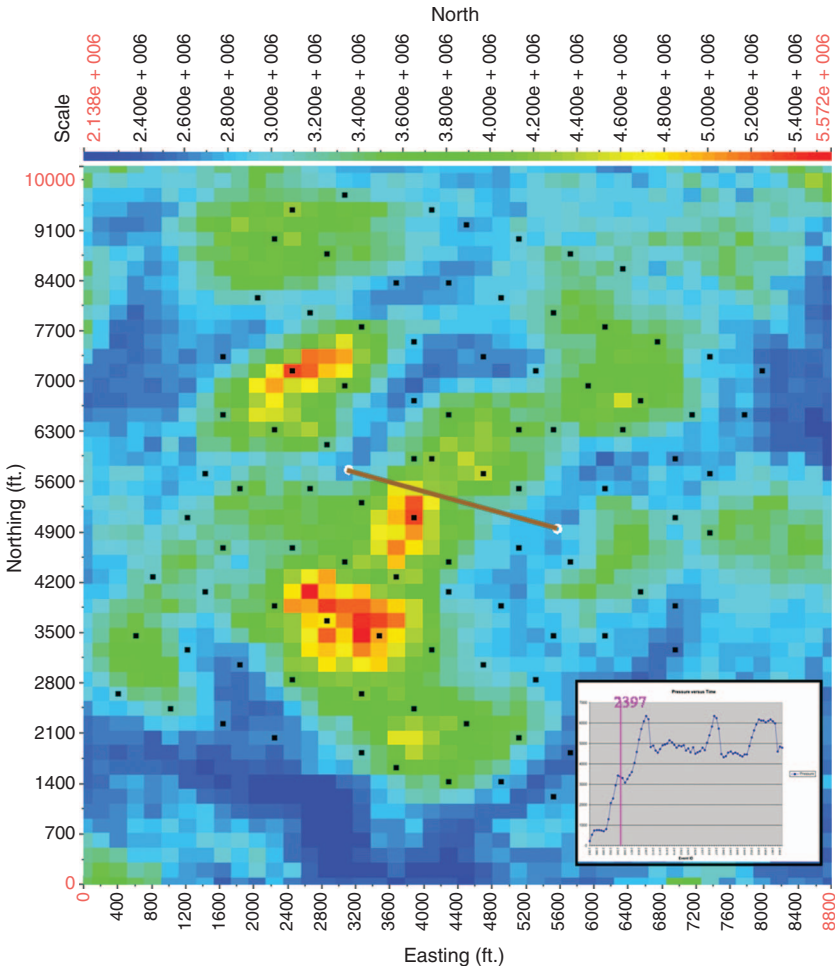

Figure 1. Depth slice at 7800 ft (2400 m) through the distribution of energy released during a 60-s interval of hydraulic-fracture stimulation of a horizontal Barnett Shale well in north Texas, as mapped with a surface array. The distribution of energy values is plotted as colored pixels, with higher energy values corresponding to warmer colors. The values on the color bar are in arbitrary units. Black dots are surface station locations. The brown line traces the position of the lateral well. The inset pressure-history curve shows the location of the sample time (minute 2397) relative to surface-measured treatment pressure. During this time, the surface pressure dropped rapidly from the local peak of 3000 psi. This 1-minute period contained the highest seismic energy seen in the early stages of pumping activity. The energy pattern traces out two northeast-southwest trends with an orientation similar to the inferred maximum horizontal stress. The northeast-southwest trend offset from the well is suspected to result from the reactivation of a pre-existing hydraulic fracture from another completed horizontal well to the north. The northeast-southwest energy near the center of the treatment well appears to be reoriented in an orthogonal direction near the southwest tip of the hydraulic fracture. This reorientation is suspected to result from the hydraulic fracture encountering a natural fracture system in the Barnett. The time at the loss of pressure corresponds to the intersection of the hydraulic fracture with the natural fracture system and is accompanied by a large release of seismic energy. From Lakings et al., 2006.

However, the common practice for reporting the result of microseismic monitoring today is to plot the estimates of the event hypocenter locations on an event-by-event basis over time. For example, Figure 2 presents the hypocenter locations for a multiwell frac in the Marcellus Shale play of Pennsylvania, U.S.A. These estimates were achieved with a single deployment of a 1428-channel star-pattern surface array (see Figure 3) over 16 mi^2 (42 km^2) for the duration of the treatment of five horizontal wells. In this analysis, no averaging over a time window has been applied; rather, the data are analyzed at the fundamental digitization rate of the field data, 2 ms. Hypocenter estimates for individual events are plotted rather than energy contours.

Several groups have developed variations on passive seismic emission tomography as described above. Kuznetsov et al. (2006) and Kochnev et al. (2007) apply long-time-interval stacking similar to semblance to detect elevated semblance (energy) over intervals of several seconds for a fixed target depth. This technique is very similar to the one that produced Figure 1. Chambers et al. (2008, 2009b) report on a study on the detectability of small events at depth with a surface array using a series of string shots of different sizes discharged at reservoir depth. The array used to capture the signals consisted of 1000 vertical geophones in 800 twelve-phone groups deployed along eight lines radiating from the wellhead like the spokes of a wheel, similar to that depicted in Figure 3. They conclude that their work demonstrates that "migration style processing methods can be used with data recorded by surface arrays to successfully image sources that are too weak to be observable in the raw data."

Downloaded 05 Dec 2010 to 99.185.9.161. Redistribution subject to SEG license or copyright; see Terms of Use at http://segdl.org/

Chambers et al. (2009a) report on their use of this migration technique to successfully image microseismic events created during hydraulic fracturing of a chalk reservoir in the Norwegian sector of the North Sea using a permanent LoFS bottom-cable array.

The work of Chambers et al. (2008, 2009a, 2009b) and similar work of Robein et al. (2009) use picking the maximum amplitude of the P-wave migrations as the imaging condition to estimate hypocenter locations. Both groups report that this approach leads to only fair vertical resolution of the located microseismic events. A method for improving this resolution is the subject of a patent granted to Duncan et al. (2008). Their method recognizes that the vertical distribution of false hypocenter estimates that result from not knowing the origin time of the event is predictable and can be used to reduce the uncertainty when selecting the true event location. Grandi and Oates (2009) crosscorrelate neighboring traces to enhance the S/N of the scattered energy and obtain higher-precision relative arrival times on all receivers.

Schisselé and Meunier (2009) show that with migration processing, it is possible to get multiple locations of the same microseismic event if the radiation pattern of the seismic signal as a result of the source mechanism of the event is such that it causes polarity changes in the signal received across a surface array. This observation suggests a problem and an opportunity. The problem is that for correct event location, the focal mechanism that created the event must be estimated and a correction for the particular radiation pattern must be applied, as done for the data in Figure 2. The opportunity is that a determination of the source mechanism conveys important information about the nature of the fractures created, as we discuss later.

Several experiments comparing the results of simultaneous surface and downhole monitoring have been reported. The results show general agreement between the event patterns detected, but timing and velocity model issues have complicated these comparisons. Lakings et al. (2006) observe agreement in trends of microseismic locations induced by hydraulic-fracture stimulation of a Barnett Shale well. Robein et al. (2009) find that the largest microseismic events imaged independently by downhole monitoring and surface array colocate subject to correction for the source mechanism of the induced microseismic events. Eisner et al. (2010a) point out that origin-time matching of the largest events provides the most reliable method of synchronization between downhole and surface catalogs and present a detailed comparison of the locations for strong mi-

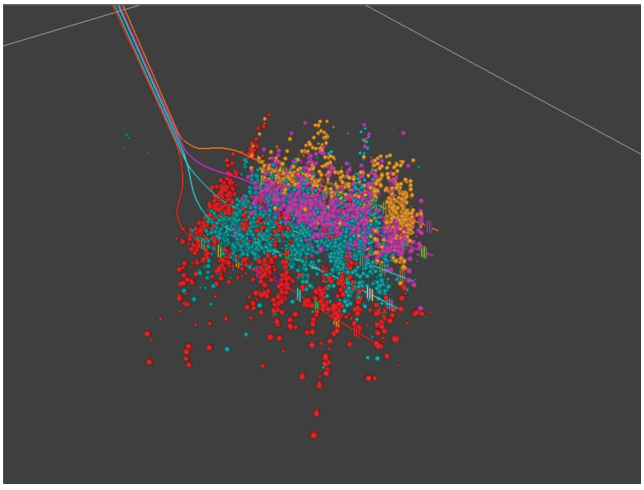

Figure 2. Perspective view of the microseismic monitoring results from treating five wells completed in the Marcellus Shale in Pennsylvania. The dots represent the estimated event hypocenters. The colors of the dots match the color of the treated well to which they correspond. The image shows the vertical portion of the wells to the left, descending from a common pad, then turning to each of the five laterals. The distance between the laterals is approximately 500 ft (150 m). The laterals are each approximately 3000 ft (1000 m) long. Courtesy Range Resources.

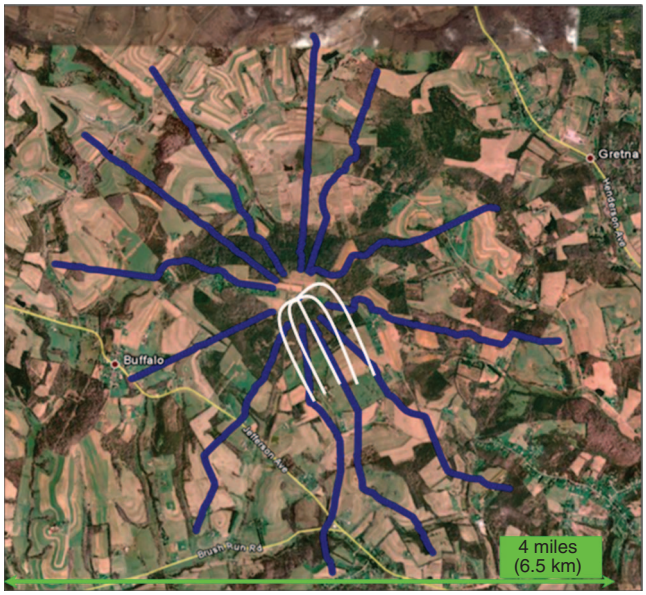

Figure 3. Map of the star-shaped layout (blue lines) for the 1428-channel surface microseismic array used to acquire the data in Figure 2. Bends in the lines are the result of obstacles or permit issues. The treatment wells are displayed in white.

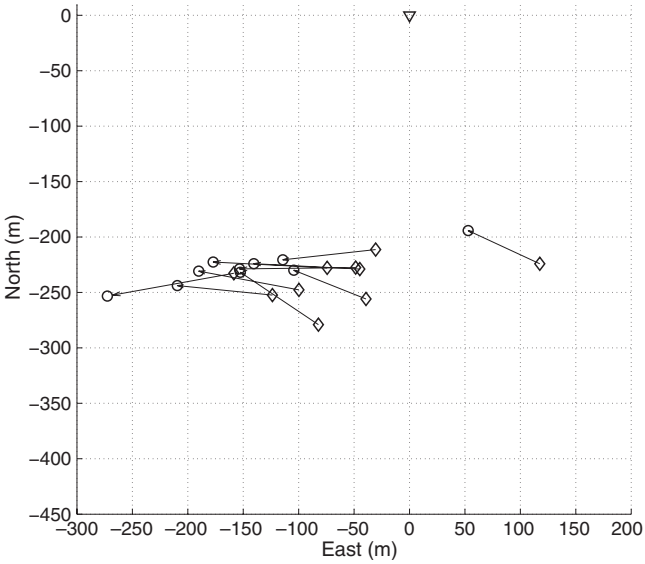

Figure 4. Map view of the 10 strongest downhole and corresponding surface-event hypocenters from monitoring a hydraulic-fracturing project observed simultaneously from the surface and downhole. Diamonds represent downhole locations; circles represent corresponding surface events found by origin time matching. The origin time match is represented by the black connecting arrows. From Eisner et al., 2010a.

Downloaded 05 Dec 2010 to 99.185.9.161. Redistribution subject to SEG license or copyright; see Terms of Use at http://segdl.org/

croseismic events, as shown in Figure 4. Downhole and surface locations are shifted relative to each other, but the east-to-west order of located events and their origin-time correspondence is evidence that the catalogs match correctly, e.g., the most westerly event from surface monitoring has the same origin time as the most westerly event from downhole monitoring. The absolute shift in locations between downhole and surface catalogs is discussed by Eisner et al. (2010a) and attributed to velocity-model errors. An integrated inversion for event locations simultaneously using surface and downhole data has not been published.

PRACTICAL FRAC MONITORING WITH SURFACE ARRAYS

Several workers have reported on surface-array monitoring of hydraulic-fracture stimulations since Duncan's (2005) and Lakings et al.'s (2006) work (e.g., Abbott et al., 2007; Kochnev et al., 2007; Barker, 2009; Hall and Kilpatrick, 2009; Keller et al., 2009; Robein et al., 2009). Almost all of these surface arrays have been deployed in a star pattern or, put another way, with the geophones, usually linear groups of vertical phones, laid out along the spokes of a wheel centered on the wellhead of the treatment well (see Figure 3). This pattern offers the best sampling of the surface noise generated by the frac pumps at the wellhead, allowing for attenuation of this noise by analog (i.e., the inherent response of a geophone group owing to its length) or digital (i.e., frequency-wavenumber) filtering. The sampling interval along the geophone lines is driven by the apparent velocity of the dominant noise. Typically, this star pattern has a diameter twice the target depth and therefore may be 2–10 km across. Consequently, a first practical consideration in performing such a survey is obtaining permits for surface access to lay out the array. Each station location must be located to submeter accuracy. Finally, layout of the typically 1000-channel array consisting of 6000–24,000 geophones requires several days from a 20–40-person crew.

Processing the data to estimate event locations involves migrating the received wavefield, as noted. A velocity model is required to achieve this imaging. A first estimate of the velocity field can be taken from available data: sonic logs or 2D or 3D seismic migration velocity fields. To achieve correct depthing, the velocity model is typically calibrated by recording a string shot at a known depth and position close to the reservoir. A string shot typically means the explosion of a length of primer cord, 20–80 ft (6–24 m) long, wrapped on a length of steel bar and lowered into the wellbore. Because the correct depth of the string shot is known, an adjustment to the average velocity can be calculated and applied so the imaged depth matches the actual. If the frac job involves perforating the casing, these perforating (perf) shots can also be used for depth calibration. It is often useful to pick residual static receiver corrections on the moveout-corrected calibration shot records. Such calibration work using various downhole sources can establish the sensitivity limits of the array in a particular location and the overall confidence in the ability of the final velocity model to place events correctly (see Chambers et al. [2008] or Hall and Kilpatrick [2009]).

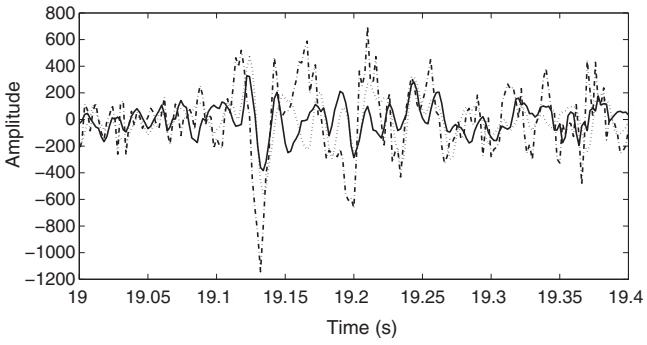

Figure 5. Particle-velocity recordings (seismic traces) of three large microseismic events (moment magnitude greater than − 1.5) as recorded on a single receiver station of a surface array while monitoring a hydraulic-fracture treatment. The events are overlain for comparison. The P-wave arrival of the three events is between 19.1 and 19.15 s. The peak direct wave has an approximately 0.03-s-long period, corresponding to an approximately 30-Hz peak period. From Eisner et al., 2010a.

An important complication to this migration procedure is that the origin times of the events are not constrained by a shot time as they are in conventional reflection seismic methods. This leads to an event-time versus event-depth interdependence that can produce ambiguity in the source location in the presence of noise. In practice, trial solutions must be made for different combinations of event-origin time and event depth. One can think of this as applying the same Kirchhoff migration operator over and over again on each trace, with each successive application moving down one sample in time. For high S/N events, the trial solution with the highest amplitude is the correct image point, ignoring the complications of radiation pattern. As noted, Duncan et al. (2008) have published a method for resolving this ambiguity in low S/N circumstances.

What we have described so far has involved the deployment of groups of vertical geophones on the surface and consequently implies P-wave imaging only. Eisner et al. (2009) discuss the uncertainties inherent in using a surface array and P-wave imaging. Uncertainties in location are driven by errors in the velocity model and by the bandwidth over which a useful signal can be extracted from the noise. Our experience is that this bandwidth is usually 10–60 Hz, as is common in land seismic techniques (see Figure 5). Eisner et al. report that the error of location in the horizontal direction has a standard deviation of 3–10 m (10–30 ft). In the vertical direction, uncertainties are typically 17–42 m (50–130 ft). With a successful depth calibration, the mean error in correct depth location relative to the calibration points is usually less than 15 m (50 ft).

One would expect that 3-C observations and shear-wave imaging in combination with P-wave imaging would improve these uncertainties. However, S-waves are greatly attenuated by the near surface (making them harder to detect), the S-wave velocity model is more problematic, and anisotropic effects are important (e.g., Kolínský et al., 2009). The effective use of S-wave imaging remains an area for future development in regard to surface and near-surface arrays.

OTHER APPLICATIONS OF SURFACE ARRAYS

In their companion paper, Maxwell et al. (2010) nicely exemplify the breadth of applications, in addition to frac monitoring, for which microseismic monitoring is relevant. These applications range from reservoir compaction to cyclic steam stimulation in heavy-oil production. They also comment on the need for integrating geologic and geomechanical considerations into the microseismic framework to achieve a proper interpretation of the data which, of necessity, begins with the location and timing of events — but should not stop there. Their comments are equally applicable to surface monitoring.

Downloaded 05 Dec 2010 to 99.185.9.161. Redistribution subject to SEG license or copyright; see Terms of Use at http://segdl.org/

Most of the surface-array work to date has been directed at frac monitoring and to a lesser extent geothermal exploration (e.g., Lees, 1998; Julian et al., 2007). Duncan (2006) shows partial results of a CO_2 injection monitoring project, and Dasgupta and Jervis (2009) report on a surface-array pilot in Saudi Arabia, designed to monitor the flood front in a water-injection project. Widespread application of the technique will require a better set of interpretation tools and procedures that will most likely be developed in the context of frac monitoring.

THE ROAD AHEAD

Neale and Smith (2009) report on a near-surface field configuration that offers several practical advantages over a purely surface array. Recognizing that the number of geophones in the surface array is primarily driven by the ambient noise levels, Neale and Smith describe a near-surface array comprised of approximately 100 stations deployed over about the same area as a star pattern with similar imaging objectives. This represents a tenfold reduction from a star-array monitor first performed in this play to confirm the surface technology. The reduced fold in the array was offset by a lower noise level, achieved by burying the geophones at each station approximately 250 ft (70 m) below the ground surface. The depth was selected after measuring the noise fall-off with depth from the surface and weighing the trade-off between drilling expense and noise reduction. This innovation was driven by the local surface conditions in a Louisiana play, which made the layout of the 1000-channel surface array extremely expensive, owing to permitting and line-cutting costs. The sparser buried array was much easier to permit because of the reduced surface impact. The cost of drilling and cementing the permanent array in place was about equivalent to laying out the surface array, but the operator ended up with a permanent facility that can be used at a small incremental cost for many future wells.

An important advantage of the permanent array is the constancy of the acquisition footprint over the life of the field, which enables a clearer picture of field development over time. Reporting on the same project, Duncan et al. (2009) note that the buried array detects more events on individual channels than the surface array, allowing for more complete source analysis, including direct-source full-moment tensor inversion (i.e., inversion from picked arrivals) on a larger fraction of the imaged events. We expect such buried arrays to account for an increasing portion of future monitoring efforts. We also expect these arrays will use more 3-C phones for full-wave recording as the joint P- and S-wave inversion methodology improves. Being below the weathering layer, these buried phones should be able to recover shear waves more effectively than a purely surface array.

Moving from acquisition to interpretation, we find several exciting developments under way as well. The first-order interpretation of microseismic data common today uses only event locations in time and space, leading to the so-called "dots in the box" display, where the hypocenter estimates are pictured as discrete spheres clustered around the treatment well. The geometry of the fractures and the volume of rock stimulated are inferred from the distribution of event locations, tempered by any knowledge of the local geology. However, if an estimate of the source mechanism of the event can be obtained from the recorded seismic data, as is routinely done in earthquake seismology, then a great deal more can be deduced. A surface (or near-surface) array provides the opportunity for an adequate sampling of the focal sphere of an event and, hence, a robust estimate of the source mechanism.

Šílený (2009) conducts a detailed study of resolution for source mechanisms using surface receivers for microseismic events with depths exceeding 4 km at the Soultz, France, geothermal field. He considers the effects of velocity mismodeling, near-surface effects, and event mislocation on networks ranging from five to as many as 29 surface stations using only P-waves or P- and S-waves. He concludes that resolution increases with the number of stations and the array aperture. Also, he concludes that the source-mechanism estimation by inverting the recorded signal is robust even with relatively large errors in the velocity model. He shows that the inverted non-double couple part of source mechanisms will be better constrained using both P- and S-waves, although the P-wave-only inversion with receivers in at least three quadrants is considered sufficiently stable.

Large networks of hundreds to thousands of receivers provide an opportunity for an even more robust source-mechanism inversion. Eisner et al. (2010b), for example, take advantage of a large (980-group) surface array, deployed for monitoring hydraulic-fracture stimulation, to estimate representative source mechanisms from the observed induced seismicity. The source mechanisms — full-moment tensor and shear-only double couple — are estimated from the surface data by a least-squares inversion of the observed P-wave amplitudes recorded on the vertical-component seismometers in the array. The moment tensor representing the source mechanism can be estimated by inverting an assumed point-source relationship between the observed displacements on the vertical component and the modeled-moment tensor components. Although in principle it is possible to use multiple wave types observed at the surface (such as P- and S-waves), using amplitudes of only direct P-waves (recorded primarily on the vertical receiver component) has the significant advantage of not projecting S-wave velocity-model errors onto the estimated source mechanisms. A sample of the seismic traces illustrating polarity reversal across the array is shown in Figure 6. The mechanism estimation can be extended to events at lower S/N levels by a relative relocation process that involves identifying a master event, then isolating events with a similar source mechanism and radiation pattern in the vicinity of the master through a crosscorrelation process (Eisner et al., 2008).

To further illustrate the point, consider that Eisner et al. (2001b) find two main sets of fault planes that fail with different mechanisms: a steeply dipping set that demonstrates normal or reverse dip-slip motion (Figure 7a and b) and a less steeply dipping set that seems to fail only with reverse motion (Figure 7c and d). Because normal and reverse motion are unlikely in the same tectonic setting, Eisner et al. postulate that the events associated with dip-slip mechanisms are most likely caused by hydraulic-fracture loading, whereas the reverse faulting along the less steeply dipping planes is more likely the result of reactivation of pre-existing faults. The map and section in Figure 8 show the distribution of dip-slip events (blue) and reverse-fault reactivation events (yellow) located in Eisner's work. The work suggests that source-mechanism characterization differentiates microseismic events that represent new fracturing as opposed to events induced on pre-existing natural faults.

To summarize, from an inversion of the source mechanism of the observed events, we gain knowledge of the strike and dip of the fracture plane, the direction of fracture motion, the type of motion (shear or tensile), and the scale of motion (moment or magnitude). Sequentially, this knowledge can be used to turn the event-location maps into a discreet fracture-network model of the stimulated reservoir, complete with flow properties suitable for reservoir simulation and production-history matching (Eisner et al., 2010b).

Downloaded 05 Dec 2010 to 99.185.9.161. Redistribution subject to SEG license or copyright; see Terms of Use at http://segdl.org/

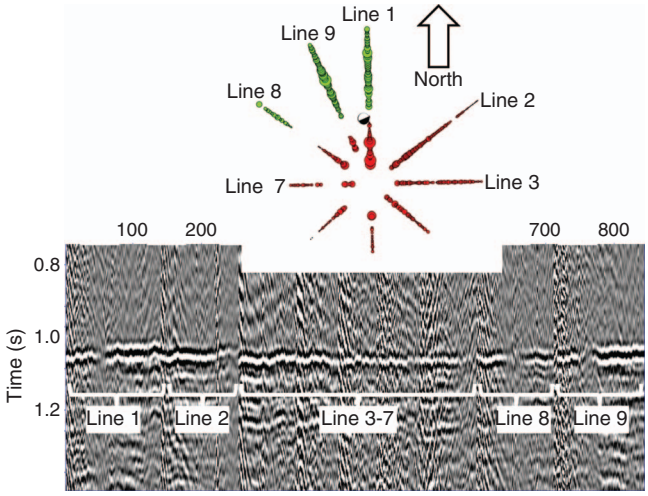

Figure 6. Variable-density plot of particle velocity for an observed microseismic event. The upper diagram shows polarity (green is upward motion, red is downward motion) and relative amplitude (circles are proportional to size of the recorded amplitudes) of the observed event at each station in the array. The focal-mechanism solution for this event is represented by the black-and-white circle (lower-hemisphere projection of the P-wave polarity) placed at the epicenter location. The event is estimated to be the result of down-to-the-south motion on a steeply dipping normal fault with east-northeast strike. The lower plot shows the corresponding scaled and moved-out vertical-component traces. Note the polarity change of the first arrival on lines 1, 8, and 9 and no polarity change on lines 2–7. Also note that the signal diminishes as receivers approach the polarity flip plane (nodal plane) on lines 1, 2, 8, and 9. Thus, at the end of line 8, the signal increases with offset because receivers are located farther away from the nodal plane. Each line has high noise levels associated with the frac pumps in the center of the star pattern. From Eisner et al., 2010b.

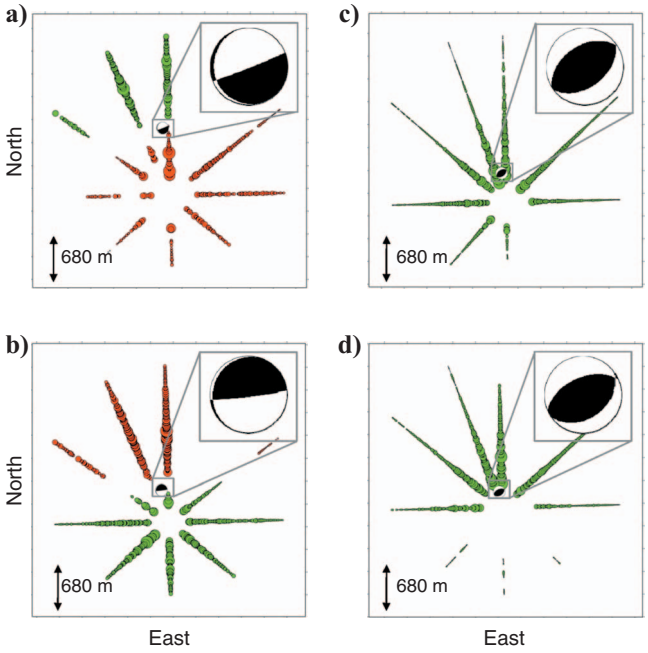

Figure 7. Polarity and relative amplitudes of first arrivals for three types of microseismic events induced during a particular hydraulic fracture stimulation. Each map is 5500×5500 m in x (east) and y (north) extent. Red circles represent downward motion, green circles represent upward motion, and circle sizes are proportional to the relative sizes of the observed amplitudes. The black-and-white circles are plotted at the microseismic event epicenters, enlarged in the corner of each plot to show details of the failure mechanism. (a, b) Steeply dipping fault-plane failures with (a) normal and (b) reverse motion. (c, d) Less steeply dipping fault-plane failures with only reverse motion. The areal extent of the amplitude and phase sampling contributes to a high-confidence source-mechanism estimate. From Eisner et al., 2010b.

Another developing area of application in which surface-array monitoring provides an opportunity is in measuring effective seismic-velocity anisotropy (the dependence of seismic velocities on the direction of propagation). Proper imaging of data acquired using a multioffset and multiazimuth distribution of receivers requires knowledge of (and provides constraints upon) the effective seismic-velocity anisotropy in the reservoir. Inversion of limited offset and azimuth data sets (such as those available from a single monitoring borehole) to estimate seismic anisotropy remains challenging, owing to its multiparameter nature and the nonuniqueness of typical anisotropy estimation problems. These difficulties usually are overcome by making certain assumptions about the anisotropic symmetry and describing the data within an assumed model such as vertical transverse isotropy (VTI). To relax those assumptions, we need more data.

One option is to supplement conventional P-wave seismic data with S-wave data (e.g., Teanby et al., 2004). Microseismic sources frequently radiate SV- and SH-waves over much larger offsets than active seismic sources can generate. Observing the travel of these phases over a large areal distribution of sensors as are available

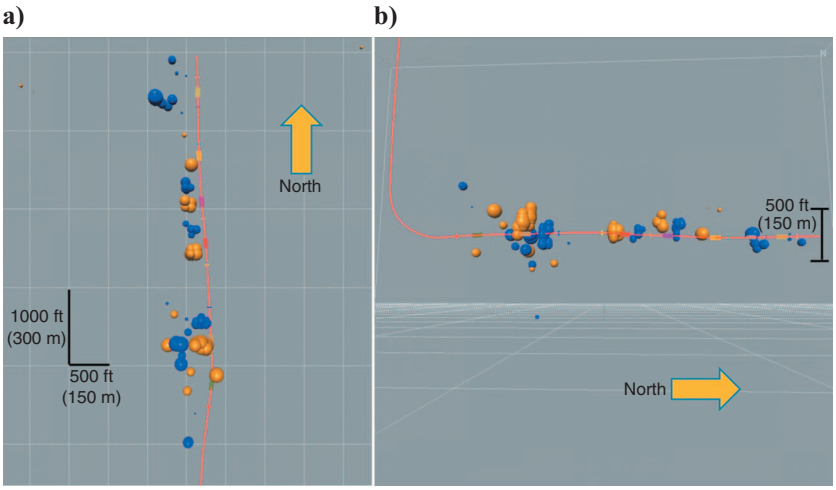

Figure 8. (a) Map view and (b) vertical cross-section depth view through mapped locations of the microseismic events in this study for which mechanisms could be determined. Two types of microseismic events are plotted: Yellow spheres correspond to the locations of the shallow-dipping, reverse-faulting events such as those in Figure 7c and d, and blue spheres correspond to locations of dip-slip events such as those in Figure 7a and b. The yellow events may represent the reactivation of pre-existing faults, and the blue events may be newly created by the frac process. Sphere size is proportional to the released seismic moment, the largest sphere representing 9.3×10^9 Nm. The treatment-well trajectory is represented by the red line. The induced events are predominantly located west of the treatment well. The dip-slip (blue) events are more confined in depth to be near the treatment well, whereas reverse-mechanism (yellow) events show significant vertical growth.

Downloaded 05 Dec 2010 to 99.185.9.161. Redistribution subject to SEG license or copyright; see Terms of Use at http://segdl.org/

with a surface array provides an excellent opportunity to measure anisotropic parameters, as discussed by Kolínský et al. (2009). In fact, Kolínský et al. note that the extent of the wavefield sample enabled by the large array allows them to conclude that a simple model (VTI) is insufficient to explain the observed shear-wave splitting.

CONCLUSIONS

The wavefield-extrapolation method to locate event hypocenters enables microseismic monitoring with surface or near-surface arrays. The method does require that a large aperture array be used to achieve sufficient resolution, and adequate fold is required to detect weak signals in the presence of noise.

The approach of using surface arrays has gained acceptance in the field of hydraulic-fracture stimulation monitoring since its introduction in 2004. Temporary monitoring using star-shaped arrays consisting of thousands of geophones on the surface is slowly giving way to monitoring with sparser permanent arrays, with sensors placed at shallow depths (about 100 m) to reduce the ambient-noise level at the individual sensors and thereby allowing for fewer sensors and lower acquisition fold. Such permanent arrays afford the opportunity to monitor more wells and treatments at a lower unit cost and more consistently over the life of the field.

Broad sampling of the energy radiated over multiple azimuths and offsets allows and requires robust estimation of the event-source mechanisms associated with the seismic signals because location and source mechanisms are joint problems in wavefield extrapolation. A solution for source mechanism in turn provides more information about the geomechanical behavior of the reservoir and how it might affect the fluid mechanics. The monitoring of several treatments on dispersed wells using the same array can also provide a very useful measure of the effective velocity anisotropy, which in turn can improve imaging by conventional reflection seismic methods. These interpretive extensions greatly increase the value proposition of microseismic frac monitoring. Application of the technique to endeavors such as hydrothermal exploration, enhanced geothermal systems, cyclic steam stimulation, CO_2 sequestration monitoring, and secondary recovery of oil and gas deposits have been made on a limited basis to date. As the interpretation of microseismic data improves in general, we would expect the range of applications to broaden.

ACKNOWLEDGMENTS

The authors would like to thank William Barker, Sherilyn Williams-Stroud, JoEllen Kilpatrick, Mike Thornton, and Brian Cornette for useful discussions and help in preparing the manuscript for this paper.

REFERENCES

Abbott, D., C. Neale, J. D. Lakings, L. Wilson, J. C. Close, and E. Richardson, 2007, Hydraulic fracture diagnostics in the Williams Fork Formation, Piceance basin, Colorado using surface microseismic monitoring technology: Proceedings of the Rocky Mountain Oil & Gas Technology Symposium, Society of Petroleum Engineers, Paper 108142.

Bailey, J. R., 1973, Mapping of earth fractures induced by hydrofracturing: U. S. Patent 3 739 871.

Barker, W., 2009, Increased production through microseismic monitoring of hydraulic fracturing over a multiwell program: Proceedings of the Annual Technical Conference and Exhibition, Society of Petroleum Engineers, Paper 124877.

Chambers, K., O. Barkved, and J.-M. Kendall, 2009a, Imaging microseismic activity using the LoFS permanent sensor surface array: 79th Annual International Meeting, SEG, Expanded Abstracts, 1612–1616.

Chambers, K., S. Brandsberg-Dahl, J.-M. Kendall, and J. Rueda, 2008, Testing the ability of surface arrays to locate microseismicity: 78th Annual International Meeting, SEG, Expanded Abstracts, 1436–1440.

Chambers, K., J.-M. Kendall, S. Brandsberg-Dahl, and J. Rueda, 2009b, The detectability of microseismic events using surface arrays: Workshop on Passive Seismic, EAGE, A25.

Claerbout, J., 1985, Imaging the earth's interior: Blackwell Scientific Publications.

Dasgupta, S. N., and M. A. Jervis, 2009, Results from passive seismic field trial for reservoir monitoring in Saudi Arabia: 71st Conference & Technical Exhibition, EAGE, Extended Abstracts, Paper X015.

Duncan, P. M., 2005, Is there a future for passive seismic?: First Break, **23**, 111–115.

——, 2006, Micro-seismic monitoring: The other 4-D: Hart E&P, **79**, 43–45.

Duncan, P. M., J. D. Lakings, and R. A. Flores, 2008, Method for passive seismic emission tomography: U. S. Patent Application Publication US 2008/0068928 A1.

Duncan, P. M., P. Smith, C. Neale, L. Eisner, and M. Thornton, 2009, A permanent geophone array for frac monitoring of the Haynesville Shale: Proceedings of the 11th Annual Unconventional Solutions Conference, Canadian Society for Unconventional Gas.

Eisner, L., D. Abbott, W. B. Barker, J. Lakings, and M. P. Thornton, 2008, Noise suppression for detection and location of microseismic events using a matched filter: 78th Annual International Meeting, SEG, Expanded Abstracts, 1431–1435.

Eisner, L., W. Heigl, P. M. Duncan, and W. Keller, 2009, Uncertainties in passive seismic monitoring: The Leading Edge, **28**, 648–655.

Eisner, L., B. J. Hulsey, P. M. Duncan, D. Jurick, H. Werner, and W. R. Keller, 2010a, Comparison of surface and borehole locations of induced seismicity: Geophysical Prospecting, doi: 10.1111/j.1365_2478.2010.00867.x.

Eisner, L., S. Williams-Stroud, A. Hill, P. M. Duncan, and M. Thornton, 2010b, Beyond the dots in the box: Microseismicity-constrained fracture models for reservoir simulation: The Leading Edge, **29**, 326–333.

Grandi, S., and S. J. Oates, 2009, Microseismic event location by cross-correlation migration of surface array data for permanent reservoir monitoring: 71st Conference & Technical Exhibition, EAGE, Extended Abstracts, X012.

Hall, M., and J. Kilpatrick, 2009, Surface microseismic monitoring of slick water and nitrogen fracture stimulations, Arkoma basin, Oklahoma: 79th Annual International Meeting, SEG, Expanded Abstracts, 1562–1565.

Julian, B. R., G. R. Foulger, and F. Monastero, 2007, Microearthquake moment tensors from the Coso geothermal area: Proceedings of 32nd Workshop on Geothermal Reservoir Engineering, Stanford University, SGP-TR-183.

Keller, W. R., B. J. Hulsey, and P. M. Duncan, 2009, Correlation of surface microseismic event distribution to water production and faults mapped on 3D seismic data: A West Texas case study: 79th Annual International Meeting, SEG, Expanded Abstracts, 1524–1526.

Kiselevitch, V. L., A. V. Nikolaev, P. A. Troitskiy, and B. M. Shubik, 1991, Emission tomography: Main ideas, results, and prospects: 61st Annual International Meeting, SEG, Expanded Abstracts, 1602–1602.

Kochnev, I. V., V. S. Polyakov, I. Murtayev, V. G. Savin, B. K. Zommer, and I. V. Bryksin, 2007, Imaging hydraulic fracture zones from surface passive microseismic data: First Break, **25**, 77–80.

Kolínský, P., L. Eisner, V. Grechka, D. Jurick, and P. M. Duncan, 2009, Observation of shear-wave splitting from microseismicity induced by hydraulic fracturing: A non-VTI story: 71st Conference & Technical Exhibition, EAGE, Extended Abstracts, X014.

Kuznetsov, O. L., L. N. Chirkina, G. A. Belova, B. Y. Meltchouk, A. S. Joukov, A. V. Volkov, V. V. Firsov, G. V. Rogotsky, I. A. Chirkin, and A. S. Voribiev, 2006, Seismic location of emission centers — A new technology for monitoring the production of hydrocarbons: 68th Conference & Technical Exhibition, EAGE, Extended Abstracts, B018 (in Russian).

Lakings, J. D., P. M. Duncan, C. Neale, and T. Theiner, 2006, Surface based microseismic monitoring of a hydraulic fracture well stimulation in the Barnett Shale: 76th Annual International Meeting, SEG, Expanded Abstracts, 605–608.

Lees, J. M., 1998, Multiplet analysis at Coso geothermal: Bulletin of the Seismological Society of America, **88**, 1127–1143.

Maxwell, S., J. Rutledge, R. Jones, and M. Fehler, 2010, Petroleum reservoir characterization using downhole microseismic monitoring: Geophysics, 75, this issue.

McMechan, G. A., 1982, Determination of source parameters by wavefield extrapolation: Geophysical Journal of the Royal Astronomical Society, **71**, 613–628.

McMechan, G. A., J. H. Luetgert, and W. D. Mooney, 1985, Imaging of earthquake sources in Long Valley caldera, California, 1983: Bulletin of

Downloaded 05 Dec 2010 to 99.185.9.161. Redistribution subject to SEG license or copyright; see Terms of Use at http://segdl.org/

the Seismological Society of America, **75**, 1005–1020.
Neale, C., and P. Smith, 2009, The use of large aperture buried geophone arrays for high efficiency stimulation and production microseismic monitoring: Annual Convention and Exhibition, AAPG, 90090.
Robein, C. E., F. Drapeau, D. L. Maurel, E. Gaucher, and E. Auger, 2009, Multi-network microseismic monitoring of fracturing jobs — Neuquen TGR application: 71st Conference & Technical Exhibition, EAGE, Extended Abstracts, X009.
Schisselé, E., and J. Meunier, 2009, Detection of micro-seismic events using a surface receiver network: Workshop on Passive Seismic, EAGE, A12.
Šílený, J., 2009, Resolution of non-double-couple mechanisms: Simulation of hypocenter mislocation and velocity structure mismodeling: Bulletin of the Seismological Society of America, **99**, 2265–2272.
Teanby, N., J.-M. Kendall, R. Jones, and O. Barkved, 2004, Stress-induced temporal variations in seismic anisotropy observed in microseismic data: Geophysical Journal International, **156**, 459–466.

Downloaded 05 Dec 2010 to 99.185.9.161. Redistribution subject to SEG license or copyright; see Terms of Use at http://segdl.org/